

Identification and optimal control of fructo-oligosaccharide production

J. Schorsch * M. Kinnaert * R. Fekih-Salem **** L. Dewasme **
C. C. Castro **** A. Vande Wouwer **

* *Department of Control Engineering and System Analysis, Université libre de Bruxelles, Belgium (e-mail: julien.schorsch, michel.kinnaert@ulb.ac.be)*

** *Automatic Control Laboratory, University of Mons, Belgium (e-mail: laurent.dewasme, radhouane.fekih-salem, alain.vandewouwer@umons.ac.be)*

*** *LAMSIN, University of Tunis El Manar, Tunisia*

**** *Applied Chemistry and Biochemistry Department, University of Mons, Belgium (e-mail: cristiana.castro@umons.ac.be)*

Abstract:

This article deals with the development of a reduced model describing the temporal evolution of the fructo-oligosaccharide production by *Aureobasidium pullulans* and the optimal process control. First, a reduced model is derived from a detailed model reproducing with good accuracy the dynamics of the fructo-oligosaccharide production. The reduced model is obtained using maximum likelihood principal component analysis and parameter identification based on a weighted least squares criterion. Next, the fructo-oligosaccharide concentration at an a priori undetermined time is maximized using Pontryagin maximum principle. The methodology is analyzed based on experimental data from batch and fed-batch cultures, and results are compared with those obtained with another simple model available in the literature.

Keywords: Pontryagin maximum principle, bang bang control, parameter estimation, biotechnology.

1. INTRODUCTION

In recent years, consumers have become increasingly concerned about processed food and have since attempted to consume healthy. To match this change in consumers' eating habits, organisations and industries developing foods for health benefit are encouraged to think differently. New research areas are hence emerging, trying to develop *characteristic functional ingredients* which confer health benefits such as dietary fiber, with prebiotic and probiotic effects (Sangeetha et al., 2005). As an example, thanks to these prebiotic effects on the human health, studies on fructo-oligosaccharides (FOS) are currently conducted.

FOS belong to the class of dietary carbohydrates. They are used as an alternative to classic sugar for their 30% relative sweetness. Moreover, they selectively increase the probiotic bacteria development resulting in the prevention of many gastrointestinal diseases, colorectal cancer, diabetes (see e.g. (Tomomatsu, 1994)). Naturally, FOS can be found in honey with a concentration of 70%, bananas as well as rye. Industrially, they are difficult to produce and several processes are required to obtain them with an acceptable degree of purity (Nobre et al., 2015, 2016).

FOS are generally produced in a bioreactor by transfructosylation of sucrose (GF) which is composed of monosaccharides glucose (G) and fructose (F), through microbial enzymes (fructosyltransferase and β -fructofuranosidase) present in microorganisms (such as *Aureobasidium pullulans* (Dominguez et al., 2012) or *Aspergillus* sp. (Rocha et al., 2009)). These enzymatic

activities produce complex sugars, namely 1-Kestose (GF₂), Nystose (GF₃) and 1-Fructofuranosyl Nystose (GF₄) which constitute the FOS family.

This paper focuses on two objectives. First, a new mathematical model is developed to reproduce the temporal evolution of the FOS production in a bioreactor operated in a fed-batch mode. From this model, an optimization method is next developed to maximize the FOS concentration.

Modeling FOS production is not straightforward and requires a good knowledge of all occurring chemical reactions. In addition to the enzymatic reactions, hydrolysis and synthesis reactions should be evaluated. Moreover, FOS production yield is affected by the generated by-products (glucose or fructose). All these constraints render difficult the development of a mathematical model since more than 7 states and a large set of unknown parameters are then required to reproduce the time evolution of FOS concentration.

A model reduction based on an existing model developed in Rocha et al. (2009); Fekih-Salem et al. (2015) is therefore proposed. It would allow the reduction of the number of parameters that need to be identified, while conserving the mass balances between each component. A two steps procedure is employed. The structure of the reduced model is first obtained by resorting to a maximum likelihood principal component analysis (MLPCA) (Mailier et al., 2013). Afterwards, the parameters are identified by using the weighted least squares (WLS) criterion. Based on the development of this model, an optimization strategy is performed to maximize the FOS concentration in a fed-batch mode.

The optimization of a fed-batch bioreactor process consists in determining the best substrate feed rate to maximize the by-product or the enzyme concentrations. Since we are faced with a singular problem in this case, the optimization is achieved by applying Pontryagin's maximum principle, and more precisely by considering a bang-bang method. This method uses the constraints on the substrate feed rate to determine the best protocol to maximize the FOS concentration (see e.g. Bryson and Ho (1969); Van Impe and Bastin (1995); Smets et al. (2004)).

Simultaneously, based on a simple second model developed in (Jung et al., 1989) and identified according to a set of experimental data, a comparison is performed to show the efficiency of the developed reduced model.

The paper is organized as follows. In Section 2, the model is presented and identified. Section 3 deals with the optimal control in order to optimize the FOS production. Both Sections are concluded by an analysis of the results. A general conclusion is delivered in Section 4.

2. MATHEMATICAL MODELS FOR FOS PRODUCTION

The development of mathematical models for FOS production has already been performed in (Jung et al., 1989; Duan et al., 1994) followed by (Rocha et al., 2009) and (Fekih-Salem et al., 2015). In the sub-figures A, B and C from Fig. 1, the associated networks of each reaction mechanisms are displayed. The first model (model A-Fig. 1) considers only the synthesis reactions of FOS by fructosyltransferase. In addition to this initial model, the Nystose hydrolysis reaction has been examined (model B-Fig. 1). The fermentative process, i.e. the biomass growth (X), and 1-Kestose and 1-Fructosylfuranosyl Nystose hydrolysis reactions are next taken into consideration (model C-Fig. 1). The latter is the most complete model and provides accurate prediction results (Rocha et al., 2009; Fekih-Salem et al., 2015). However, because of its complexity in terms of the number of chemical reactions, namely 7 Michaelis-Menten laws augmented with/without substrate inhibition and/or competitive glucose inhibition and 2 Monod laws, 41 unknown parameters have to be identified.

Ideally, the available data obtained from the experiments are continuously measured. In this situation, it would be possible to avoid the identifiability problem and provide unbiased estimates, even with 41 parameters to be identified. However, in real applications, the data is sampled and each experimental sample has to be collected carefully without affecting the enzymatic and biological reactions. Respecting these conditions, only one sample around every 5 hours is accessible in the FOS case. This lack of data increases the uncertainties of the estimated parameters. Such a situation has already been observed for the identification of the complete model C in (Fekih-Salem et al., 2015). To decrease these uncertainties, a solution is to create a new model by reducing the complete model. The latter is compared with the simple model developed by Jung et al. (1989).

The identification of both models is performed from a combination of experiments: 2 in batch and 2 in fed-batch for different initial conditions of sucrose. The enzymatic reactions have been obtained from *Aureobasidium Pullulans* where the experimental conditions are described in Fekih-Salem et al. (2015).

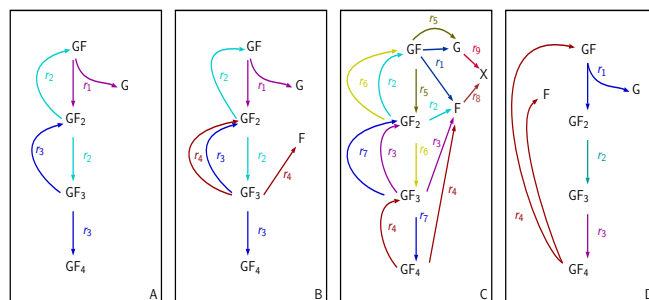


Fig. 1. Network of the reaction mechanisms; A: Jung et al. model Jung et al. (1989); B: Kow et al. model Duan et al. (1994); C: Rocha et al. model Rocha et al. (2009); D: proposed model. Each color represents a reaction rate.

2.1 Model reduction

Using a MLPCA approach detailed in (Mailier et al., 2013), we are able to determine the minimum number of reactions likely to explain the noisy data and the related stoichiometric matrix. The model C developed in (Rocha et al., 2009) involving 8 state variables and 41 parameters is reduced to a 7 state variables and 14 parameters model. Such model simplification has been carried out through a step by step parameter identification procedure:

- determine an initial reaction stoichiometry using MLPCA;
- estimate the kinetic parameters using weighted least squares;
- compute the parameter confidence intervals and correlations and eliminate highly correlated parameters from the model;
- iterate the identification procedure questioning the stoichiometry and kinetics.

The value of this procedure is to segment the original problem into subproblems that can be initiated by the solution of previous steps. More precisely, the final reduced model has 8 Kinetic parameters and 6 pseudo-stoichiometric coefficients and the differential equation system is as follows:

$$\begin{cases} \dot{[GF]} &= -r_1 + k_{14}r_4 + \frac{1}{V}([GF]_{in} - [GF])Q \\ \dot{[GF_2]} &= -r_2 + k_{21}r_1 - \frac{[GF_2]}{V}Q \\ \dot{[GF_3]} &= -r_3 + k_{32}r_2 - \frac{[GF_3]}{V}Q \\ \dot{[GF_4]} &= -r_4 + k_{43}r_3 - \frac{[GF_4]}{V}Q \\ \dot{[F]} &= k_{54}r_4 - \frac{[F]}{V}Q \\ \dot{[G]} &= k_{61}r_1 - \frac{[G]}{V}Q \\ \dot{V} &= Q \end{cases} \quad (1)$$

$[\alpha]$ denotes the concentration (in g.L^{-1}) of the component α . Q represents the substrate feed rate (in L.h^{-1}), also denoted control input variable. $[GF]_{in}$ is the substrate concentration (in g.L^{-1}). The V variable is the volume (in L) of the broth inside the vessel of the bioreactor. The reaction rates (in $\text{g.L}^{-1}.\text{h}^{-1}$) are defined by the Monod-law

$$r_i = \mu_i^{\max} \frac{[GF_i]}{K_{m_i} + [GF_i]}, \text{ with } i = 1, 2, 3, 4, \quad (2)$$

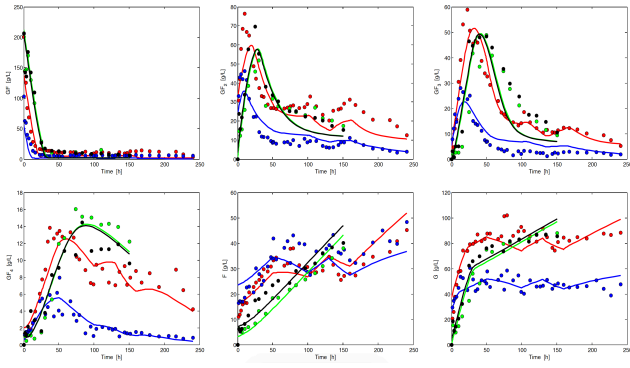
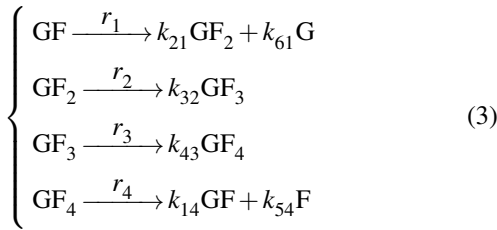


Fig. 2. Measurements (dotted line) and simulations (continuous lines) from model (1) with 8 kinetic parameters and 6 stoichiometric parameters. Blue and red colors represent the fed-batch runs, and green and black colors show the batch runs.

where μ_i^{\max} denotes the maximum rate (in $\text{g.L}^{-1}.\text{h}^{-1}$) of the reaction i . K_{m_i} (in g.L^{-1}) represents the half-saturation Michaelis-Menten constant associated with the component i . The associated reaction scheme is given by

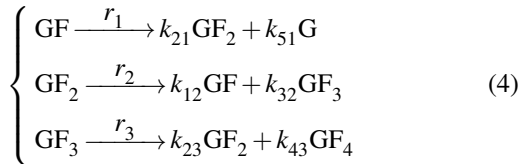


The network of the reaction mechanisms is shown in (D-Fig. 1). Because of its limited impact on the FOS concentration, the growth of the biomass is not taken into consideration in this reduced model.

The estimated parameters, the confidence intervals as well as the root mean-square error (RMSE) are displayed in Table 1. The standard deviations are relatively small with respect to the estimated parameters. The 4 experimental data sets and the corresponding model (1) prediction are plotted in Fig. 2. It can be noticed that the model satisfactorily fits the data which validates the obtained results.

2.2 Jung et al. Model

The reaction scheme proposed by Jung et al. Jung et al. (1989) is given by



where the time evolution of the concentrations is described by

$$\left\{ \begin{array}{l} \dot{[\text{GF}]} = -r_1 + k_{12}r_2 + \frac{1}{V}([\text{GF}]_{\text{in}} - [\text{GF}])Q \\ \dot{[\text{GF}_2]} = -r_2 + k_{21}r_1 + k_{23}r_3 - \frac{[\text{GF}_2]}{V}Q \\ \dot{[\text{GF}_3]} = -r_3 + k_{32}r_2 - \frac{[\text{GF}_3]}{V}Q \\ \dot{[\text{GF}_4]} = k_{43}r_3 - \frac{[\text{GF}_4]}{V}Q \\ \dot{[\text{G}]} = k_{51}r_1 - \frac{[\text{G}]}{V}Q \\ \dot{V} = Q \end{array} \right. \quad (5)$$

In this case, the reaction rate r_1 is given by a modified Michaelis-Menten law describing the competitive glucose inhibition

$$r_1 = \mu_1^{\max} \frac{[\text{GF}]}{K_{m_1} + [\text{GF}] + K_{m_1}/K_G[\text{G}]} \quad (6)$$

The parameter K_G is the competitive inhibition constant (in g.L^{-1}) for glucose. The reaction rates r_2 and r_3 are given by the following Michaelis-Menten laws

$$r_2 = \mu_2^{\max} \frac{[\text{GF}_2]}{K_{m_2} + [\text{GF}_2]}, \quad r_3 = \mu_3^{\max} \frac{[\text{GF}_3]}{K_{m_3} + [\text{GF}_3]} \quad (7)$$

This model consists in 7 kinetic parameters (μ_i^{\max} , K_{m_i} for $i = 1, 2, 3$ and K_G) and 6 pseudo-stoichiometric k -coefficients that have to be identified.

Notice that, for simplicity, the nomenclature for both models are the same.

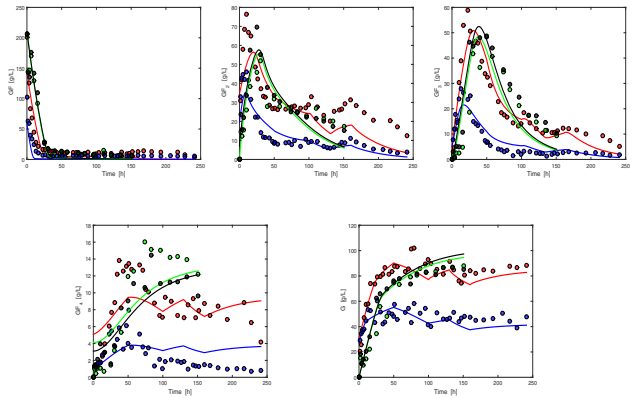


Fig. 3. Measurements (dotted lines) and simulations (continuous lines) from model (5) with 7 kinetic parameters and 6 stoichiometric parameters. Blue and red colors represent the fed-batch runs, and green and black colors show the batch runs.

The estimated parameters are obtained using weighted least squares, in the same spirit as in the previous subsection. The confidence intervals and the RMSE are displayed in Table 1. Fig. 3 shows that the model (5) adequately reproduces the experimental data in 2 batch and 2 fed-batch culture mode for most of the state variables. In Fig. 4, model trajectories of (5) are complemented by their related 95%-confidence corridors. All the experimental samples have a non-empty intersection with the 95%-confidence intervals of the simulated concentrations. This result illustrates the good fitting of experimental data and the accuracy of the estimated parameters.

2.3 Discussion 1

In this study, two models are selected to reproduce the FOS concentration evolution. These models are easier to identify than the complex model detailed in (Rocha et al., 2009) and require low computational effort for emulation. The latter consideration is advantageous when considering optimal control.

The reduced model (1) and the identified Jung's model (5) both accurately reproduce the experimental data. However, the reduced model, where the structure has been obtained using MLPCA, is the most appropriate since 4 reaction rates are considered to determine the temporal dynamics. Thanks to the

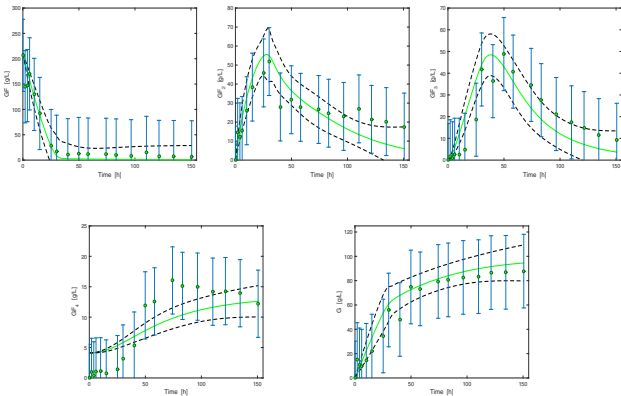


Fig. 4. The 95%-confidence corridors related to the model (5) for a control set of experimental data obtained in batch mode. The green dots with blue error bars represent the experimental samples. The green solid and black dashed lines are the simulated concentrations and the 95%-confidence intervals respectively.

Table 1. Parameter identification results of models (1) and (5) in 2 batch -2 fed-batch culture mode.

Model (1)		Model (5)		Unit
Name	Estimated	Name	Estimated	
μ_1^{\max}	9.11 ± 0.31	μ_1^{\max}	9.5 ± 1.12	$\text{g}_{\text{GF}_1} \cdot \text{L}^{-1} \cdot \text{h}^{-1}$
μ_2^{\max}	7.13 ± 0.17	μ_2^{\max}	58.02 ± 3.19	$\text{g}_{\text{GF}_2} \cdot \text{L}^{-1} \cdot \text{h}^{-1}$
μ_3^{\max}	7.91 ± 0.12	μ_3^{\max}	9.69 ± 0.32	$\text{g}_{\text{GF}_3} \cdot \text{L}^{-1} \cdot \text{h}^{-1}$
μ_4^{\max}	0.25 ± 0.01			$\text{g}_{\text{GF}_4} \cdot \text{L}^{-1} \cdot \text{h}^{-1}$
		K_G	0.3 ± 0.06	$\text{g}_G \cdot \text{L}^{-1}$
K_{m1}	12.03 ± 7.89	K_{m1}	0.039 ± 0.05	$\text{g}_{\text{GF}_1} \cdot \text{L}^{-1}$
K_{m2}	140.2 ± 12.5	K_{m2}	592.4 ± 124.6	$\text{g}_{\text{GF}_2} \cdot \text{L}^{-1}$
K_{m3}	24.8 ± 8.9	K_{m3}	39.46 ± 16.22	$\text{g}_{\text{GF}_3} \cdot \text{L}^{-1}$
K_{m4}	1.37 ± 0.59			$\text{g}_{\text{GF}_4} \cdot \text{L}^{-1}$
k_{14}	5.52 ± 0.76	k_{12}	0.54 ± 0.24	
k_{21}	0.44 ± 0.03	k_{21}	0.49 ± 0.07	
k_{32}	3.04 ± 0.36	k_{23}	0.37 ± 0.15	
k_{43}	0.09 ± 0.01	k_{32}	1.27 ± 0.34	
k_{54}	1.27 ± 0.11	k_{43}	0.019 ± 0.0045	
k_{61}	0.25 ± 0.02	k_{51}	0.23 ± 0.05	
RMSE	8.18	RMSE	8.71	

backward reaction rate r_4 , this latter model emulates more precisely the time evolution of GF_4 . On the contrary, the model initially developed by Jung et al. Jung et al. (1989) does not take into consideration this backward reaction, explaining a lower level of accuracy in the simulation of GF_4 with this model, see Fig. 5.

3. OPTIMIZATION OF FOS PRODUCTION

The aim of this section is to determine an optimal substrate feed rate for optimizing the FOS concentration at an undetermined final time. The feed profile implies the adjustment of different issues, such as feeding starting time, feeding rate or again feeding stopping time. Resorting to Pontryagin's maximum principle in the framework of singular control problem, the optimal feed rate is here adjusted.

3.1 Pontryagin's maximum principle

Both models (1) and (5) can be considered in the general nonlinear form provided by

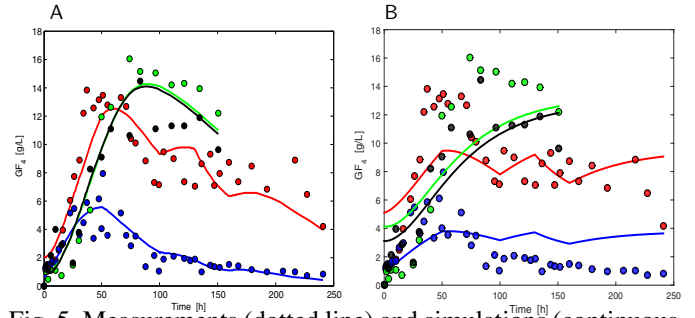


Fig. 5. Measurements (dotted line) and simulations (continuous line) from models (1) (subplot A) and (5) (subplot B). Blue and red colors represent the fed-batch realization, and green and black colors show the batch case.

$$\frac{dX}{dt} = f(X) + g(X)Q \text{ with } t_0 \leq t \leq t_f \quad (8)$$

with $X(t)$ the state vector ($X = [\text{GF}_1, \text{GF}_2, \text{GF}_3, \text{GF}_4, F, G, V]$). The function f represents the dynamics of the chemical process while g determines the fed-batch dynamics. t is the time variable (in h), t_0 and t_f represent the initial and the final time values respectively. At $t = t_0$ the system is subjected to the initial condition $X(t_0) = X_0$. The final condition is provided by

$$\Omega = V(t_f) - V_{\max} = 0. \quad (9)$$

This latter condition determines the vessel volume of the bioreactor at the final time t_f . V_{\max} represents the effective maximal volume (in L).

The performance index, J , to be maximized is a function of X defined by

$$J(t_f) = [\text{GF}_2](t_f) + [\text{GF}_3](t_f) + [\text{GF}_4](t_f) \equiv h(X), \quad (10)$$

it is the sum of the concentration of the FOS components at the final time. Notice that the model is affine in the control variable Q and the performance index is independent from the latter.

The substrate feed rate Q is limited by the feed pump capacity. Let Q_{\max} and Q_{\min} be the upper and lower capacities respectively, the function Q is bounded by

$$Q_{\min} \leq Q \leq Q_{\max}. \quad (11)$$

The objective is to find an admissible control function, $Q(t)$, which yields an admissible trajectory for the system (8) and which satisfies (9) and (11) while maximizing the performance index J .

The classical maximum principle of Pontryagin is employed to solve this problem. Maximizing the Hamiltonian H defined below, is the same as maximizing the performance index (10) (as introduced for instance in (Bryson and Ho, 1969))

$$H = \phi + \psi Q \quad (12)$$

where the functions ϕ and ψ are respectively given by

$$\phi = \lambda^\top f(X) \text{ and } \psi = \lambda^\top g(X). \quad (13)$$

The vector λ is called costate vector and has the same dimensions as X . It is defined by

$$\frac{d\lambda^\top}{dt} = -\frac{\partial H}{\partial X} = -\lambda^\top \frac{\partial f}{\partial X} - \lambda^\top \frac{\partial g}{\partial X} Q. \quad (14)$$

The general transversal conditions are given by

$$\lambda(t_f) = \frac{\partial h(X)}{\partial X} + v \frac{\partial \Omega(X)}{\partial X} \quad (15)$$

which provide $\lambda_{GF,G,F}(t_f) = 0$, $\lambda_{GF_2,GF_3,GF_4}(t_f) = 1$ and $\lambda_v(t_f) = v$ with $v \in \mathbb{R}$ where λ_α is the costate associated to the state α .

We can observe that the Hamiltonian (12) is affine in the control input. In general, no maximum exists in this context. However, because of the linear inequality constraints on the control variable, corresponding to the hardware constraints, a solution exists by resorting to the bang-bang method with singular arcs. This method consists in evaluating the sign of the partial derivative of the Hamiltonian with respect to Q , i.e. the value of ψ :

$$\begin{cases} \text{if } \psi < 0, \text{ then } Q = Q_{\min}, \\ \text{if } \psi = 0, \text{ then } Q = Q_s, \\ \text{if } \psi > 0, \text{ then } Q = Q_{\max}. \end{cases} \quad (16)$$

Q_s is called singular control law. It is obtained by taking the second time derivative of ψ (see e.g. Bryson and Ho (1969)), which yields

$$Q_s = -\frac{\lambda^\top \left(\frac{\partial q}{\partial x} f - \frac{\partial f}{\partial x} q \right)}{\lambda^\top \left(\frac{\partial q}{\partial x} g - \frac{\partial g}{\partial x} q \right)} \quad (17)$$

under the condition that $\lambda^\top \left(\frac{\partial q}{\partial x} g - \frac{\partial g}{\partial x} q \right) \neq 0$, where q is defined by

$$q = \frac{\partial g}{\partial x} f - \frac{\partial f}{\partial x} g. \quad (18)$$

This criteria is based on the necessary optimality conditions which include

$$\frac{\partial H}{\partial Q} = \lambda^\top g = 0. \quad (19)$$

Based on this development, an algorithm is now detailed.

3.2 Algorithm

The algorithm is composed of 5 steps. The first step corresponds to the initialization part. Next, a first loop is achieved to estimate the unknown coefficient v . This coefficient has a significant impact on the final volume. Finally, a second loop is achieved to determine the optimal time horizon t_f in the cost function J .

- (1) Guess t_f , v and a substrate feed rate Q respecting the final condition (9), and integrate forward the model defined by Equation (8).
- (2) Determine λ by integrating backward Equation (14).
- (3) Integrate forward the model defined in Equation (8) using singular control (16).
- (4) Repeat Steps 2 and 3, considering $v = v + \delta v$, with δv as small as required, until $\Omega = 0$.
- (5) Repeat Steps 2 to 3 with a new guess of t_f in order to maximize the cost function J defined in (10) and push the Hamiltonian (12) to zero.

The final time t_f is increased as long as the obtained FOS concentration profile is monotonically increasing. On the other hand, if a maximum is observed, t_f is decreased in order to stop the operation when the maximum is reached.

3.3 Results

The models detailed in Equations (1) and (5) are used for optimizing the FOS production. The initial conditions and set points used in the process models are referenced in Table 2.

Table 2. Optimal control: hardware constraints and initial conditions.

Hardware constraints		Initial conditions	
GF_{in}	280 g.L ⁻¹	$[GF](t_0)$	200 g.L ⁻¹
V_{max}	3 L	$V(t_0)$	1 L
Q_{max}	0.5 L.h ⁻¹	$[G](t_0)$ and $[F](t_0)$	0 g.L ⁻¹
Q_{min}	0 L.h ⁻¹	$[GF_{2,3,4}](t_0)$	0 g.L ⁻¹

For both models, the optimal substrate feed rate is equivalent (subplot A in Figs. 6). First, the feed rate reaches its upper boundary $Q_{max} = 0.5 \text{ L.h}^{-1}$ until the vessel of the bioreactor is filled up. After 4 hours of feeding, the bioreactor operates in a batch mode, where no substrate is added $Q_{min} = 0 \text{ L.h}^{-1}$. This profile allows to maximize the productivity of GF_2 which is directly linked to the substrate concentration GF . This phenomenon is shown on the subplot B of Figs. 6 by displaying the corresponding reaction rate r_1 .

For the first model described by Equation (1), the time evolution of r_1 approaches without meeting its maximum rate μ_1^{max} . A bigger substrate concentration GF_{in} should then be required to maximize this reaction. However, the global reaction rate, defined by $f_{GF_2} + f_{GF_3} + f_{GF_4}$, keeps increasing after the feeding time and reaches its maximum after 10 hours (see subplot C in Fig. 6).

Concerning the second model (5), the reaction rate r_1 reaches its maximum involving a maximal global reaction rate (subplot C in Fig. 6). The global reaction rate starts to decrease once the bioreactor is no longer fed.

Regarding the FOS concentration, the reduced model (1) provides a 125 g.L⁻¹ FOS concentration after 45.4 hours. The productivity and the yield (given in Equation (20)) are $\mathcal{P}(t_f) = 2.75 \text{ g.L}^{-1} \cdot \text{h}^{-1}$ and $\mathcal{Y}(t_f) = 49.3\%$ respectively.

$$\begin{cases} \mathcal{P}(t_f) = \frac{[GF_2](t_f) + [GF_3](t_f) + [GF_4](t_f)}{t_f}, \\ \mathcal{Y}(t_f) = V_{max} \frac{[GF_2](t_f) + [GF_3](t_f) + [GF_4](t_f)}{[GF](t_0)V(t_0) + GF_{in}(V_{max} - V(t_0))}. \end{cases} \quad (20)$$

The model developed by Jung et al. (5) gives at the final time 40.3 hours a 118 g.L⁻¹ FOS concentration, $\mathcal{P}(t_f) = 2.92 \text{ g.L}^{-1} \cdot \text{h}^{-1}$ and $\mathcal{Y}(t_f) = 46.5\%$.

3.4 Discussion 2

Based on the two models identified in Section 2, an optimization method to maximize the FOS concentration has been here proposed. Using the Pontryagin's maximum principle, the optimal substrate feed rate is similar in both cases. First, the bioreactor is filled. Secondly, the bioreactor operates in a batch mode. This profile allows to maximize the reaction rate generating GF_2 and then to promote the other reaction rates. A FOS concentration of 121.5 g.L⁻¹ for an average time of 42.85 hours should be obtained.

These results show that the reduced model, developed in this paper, is then well adapted for determining the optimal substrate feed rate necessary to optimize the FOS concentration. Moreover, this model is able to emulate more accurately each components of the FOS concentration than the simple model. Accurate knowledge of the concentration of each FOS is important for the study of the FOS separation, which can notably be performed by simulated moving-bed chromatography Nobre et al. (2016). Therefore the new model is believed to be superior

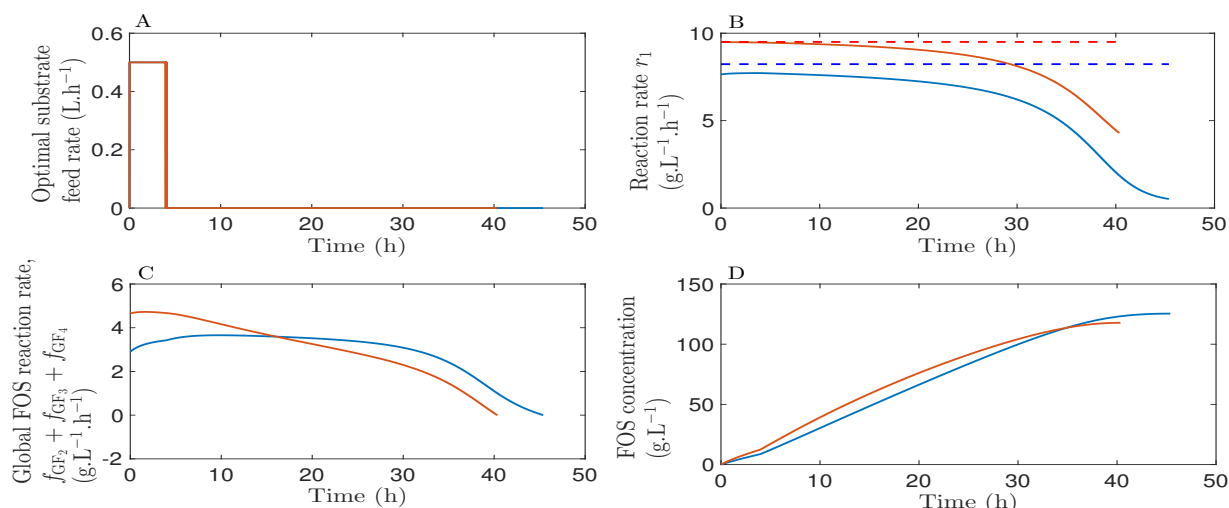


Fig. 6. The blue and red colors correspond to the results obtained from the reduced model (1) and the simple model (5) respectively. In subplot A the optimal substrate feed rate is plotted. Subplot B shows the reaction rates r_1 (continuous line) and the associated maximum rates (dotted line). The global FOS production rate is displayed in subplot C. In subplot D presents the evolution of FOS concentrations.

to the simple model with regard to the study of the global FOS production process.

4. CONCLUSION

A new approach for modeling and optimizing FOS production has been presented. It consists in reducing an existing complex model to simplify the identification and decrease the uncertainty on the parameters. It allows to accurately reproduce experimental data. From this model, an optimization procedure has been developed to maximize the FOS concentration on the basis of which an experimental protocol has been proposed.

ACKNOWLEDGEMENTS

This paper presents research results of the Belgian Network DYSCO (Dynamical Systems, Control, and Optimization), funded by the Interuniversity Attraction Poles Programme initiated by the Belgian Science Policy Office. The authors also gratefully acknowledge the financial support from the F.R.S.-FNRS, the Belgium National Fund for the Scientific Research, (PDR: T.0196.13).

REFERENCES

Bryson, A.E. and Ho, Y.C. (1969). *Applied optimal control*. Ginn and Co, Waltham, Mass.

Dominguez, A., Nobre, C., Rodrigues, L.R., Peres, A.M., Rocha, I., Lima, N., and Teixeira, J.A. (2012). New improved method for fructooligosaccharides production by *aureobasidium pullulans*. *Carbohydrate Polymers*, 89(4), 1174–1179.

Duan, K.J., Chen, J.S., and Sheu, D.C. (1994). Kinetic studies and mathematical model for enzymatic production of fructooligosaccharides from sucrose. *Enzyme Microb. Technol.*, 334–339.

Fekih-Salem, R., Vande Wouwer, A., De Castro, C., Nobre, C., and Hanstson, A.L. (2015). Parameter identification of the fermentative production of fructo-oligosaccharides by *aureobasidium pullulans*. In *Proceedings of the 19th International conference on system theory, control and computing*, 43–48.

Jung, K., Run, J.W., Kang, K.R., Lim, J.Y., and Lee, J.H. (1989). Mathematical model for enzymatic production of fructo-oligosaccharides from sucrose. *Enzyme Microb. Technol.*, 11, 491–494.

Mailier, J., Remy, M., and Vande Wouwer, A. (2013). Stoichiometric identification with maximum likelihood principal component analysis. *J. Math. Biol.*, 67, 739–765.

Nobre, C., Castro, C., Hantson, A.L., Teixeira, J., De Weireld, G., and Rodrigues, L. (2016). Strategies for the production of high-content fructo-oligosaccharides through the removal of small saccharides by co-culture or successive fermentation with yeast. *Carbohydrate polymers*, 136, 274–281.

Nobre, C., Teixeira, J.A., and Rodrigues, L.R. (2015). New trends and technological challenges in the industrial production and purification of fructo-oligosaccharides. *Critical Reviews in Food Science and Nutrition*, 55, 1444–1455.

Rocha, O., Nobre, C., Dominguez, A., Torres, D., Faria, N., Rodrigues, L., Teixeira, J.A., Ferreira, E.C., and Rocha, I. (2009). A dynamical model for the fermentative production of fructooligosaccharides. *Computer Aided Chemical Engineering*, 27, 1827–1832.

Sangeetha, P.T., Ramesh, M.N., and Prapulla, S.G. (2005). Recent trends in the microbial production, analysis and application of fructooligosaccharides. *Trends in food science & technology*, 16, 442–457.

Smets, I.Y., Claes, J.E., November, E.J., Bastin, G.P., and Van Impe, J.F. (2004). Optimal adaptive control of (bio)chemical reactors: past, present and future. *Journal of Process Control*, 14, 795–805.

Tomomatsu, H. (1994). Health effects of oligosaccharides. *Food Technol*, 48, 61–65.

Van Impe, J.F. and Bastin, G. (1995). Optimal adaptive control of fed-batch fermentation processes. *Control Eng. Practice*, 3(7), 939–954.